Pollution simulations and in-field measurements performed in March at Longyearbyen, Spitzbergen

Albert Oliver-Serra[2][0000-0002-3783-8670], Leszek Siwik[1][0000-0003-0535-7220], Natalia Leszczyńska[3][0009-0009-5210-3144], Maciej Sikora[1][0009-0006-4465-2395], Tomasz Maciej Ciesielski[4][0000-0001-7509-1662], Eirik Valseth[5,6,7][0000-0001-6940-4191], Jacek Leszczyński[1][0000-0001-7512-994X], Anna Paszyńska[1][0000-0002-0716-0619], Maciej Paszyński[1][0000-0001-7766-6052]

[1]AGH University of Krakow, Poland
[2]The University of Las Palmas de Gran Canaria, Spain
[4]The University Centre in Svalbard, Longyearbyen, Norway
[5]Oden Institute for Computational and Engineering, USA
[6]Simula Research Laboratory, Oslo, Norway
[7]Norwegian University of Life Sciences, As, Norway
albert.oliver@ulpgc.es, siwik@agh.edu.pl, s82950@365.sum.edu.pl, maciejsikora@agh.edu.pl, tomaszc@unis.no, evalseth@gmail.com, jale@agh.edu.pl, apaszynska@agh.edu.pl, paszynsk@agh.edu.pl

Abstract. Spitzbergen is Norway's largest island, located in the Svalbard archipelago of the Polar Circle region. The island's population is currently about two and a half thousand, and it works mainly in natural resource extraction, tourism, and scientific research. The subject of our interest is the town of Longyearbyen, the capital of Spitzbergen, with a population of about 1,800. It has an airport and, until recently, the only power plant in Norway that generated electricity by burning coal. The coal has been replaced recently with diesel generators to reduce the pollution output, but the problem is still there. In this paper, we present the hypergraph grammar-based model of mesh generation and finite element pollution propagation simulations at Svalbard at Spitzbergen. We also perform in-field pollution measurements with snowmobiles. The simulations and measurements have been performed in March 2024. We compare our simulation results with in-field measurements.

Keywords: Outdoor air quality at Longyearbyen, Spitzbergen, Finite element simulations, Global Wind Atlas, Hypergraph transformations

1 Introduction

The island of Spitzbergen, located in the Svalbard archipelago, has two permanently inhabited towns, Longyearbyen and Barentsburg. The archipelago residents mostly engage in scientific research, coal mining, and tourism. The capital

ICCS Camera Ready Version 2025
To cite this paper please use the final published version:
DOI: 10.1007/978-3-031-97635-3_42

of Svalbard is the town of Longyearbyen, with a population of about 2,000. It is home to an airport and formerly Norway's only coal-fired power plant, recently replaced by diesel generators. In Longyearbyen, there is also the University Centre in Svalbard (UNIS), the northernmost university in the world, where Arctic Biology, Geology, Geophysics, Technology, and Arctic Safety are the subjects of teaching and research. The Longyearbyen region is also home to the famous seed vault [3]. Longyearbyen is located in the bay of Isfjorden, the second-largest fjord in Svalbard. The town has a location in the valley (see Fig.1) favorable for a specific local microclimate. There are only two unique seasons on Svalbard. The first is the polar night, which lasts about two and a half months, during which the sun does not rise at all, and night reigns throughout. The polar night begins with a long twilight and ends with a long morning, during which the sun is below the horizon line for days. Between March and October, the sun rises for several hours a day, for about 2 hours in March and October, to a maximum of 8 hours in August.

Fig. 1: Topography of Longyearbyen at Spitzbergen. Source: https://toposvalbard.npolar.no, permission to use in article granted in terms of service at courtesy of Norwegian Polar Institute. Snowmobiles and the air quality sensor used to take the ($PM_{2.5}$) concentration measurements in Svalbard on 17/03/2024.

Air pollution in Longyearbyen was generated by a coal-fired power plant, recently replaced by diesel generators. During a normal day, due to thermal inversion effects in the morning, the air and pollutants are kept at ground level. When the rising sun subsequently warms the air mass, the layer of fog and pollution is lifted up and dispersed. This air convection process is important for this region's (broadly understood) inhabitants since their exposure to dangerous pollutants is significantly decreased.

In this paper, we perform computer simulations of the propagation of pollution generated by power plants, and we compare them with in-field measurements from snowmobiles, which were performed in March 2024. For the simulations of the pollution propagation from the power plant, we employ a finite element solver with the advection-diffusion model [11] stabilized with the Streamlined-Upwind-Petrov-Galerkin (SUPG) method [2]. The generation and processing of the computational grids for 3D finite element method simulations is a compu-

ICCS Camera Ready Version 2025
To cite this paper please use the final published version:
DOI: 10.1007/978-3-031-97635-3_42

tationally intense task. We employ the hypergraph-grammar model of the 3D longest edge refinement algorithm. The longest-edge refinement algorithm has been initially proposed for 2D meshes by Cecilia Rivara [12,13]. The hypergraph grammar-based mesh refinements for 2D grids have been employed and discussed in [11], and in [7,8,9,10] with the hanging nodes version. In this paper, we present a novel hypergraph grammar-based model of mesh transformations expressing the 3D longest-edge refinement algorithm.

2 In-field measurements

Snowmobiles are the second most important source of air pollutants (and of ($PM_{2.5}$) in particular) in the Svalbard area. The negative impact of snowmobiles on (local) air quality has been considered by some researchers and environmental agencies, in particular concerning arctic regions [5]. There are 3000 snowmobiles registered at Svalbard between 1974-2024. To understand the impact of these snowmobiles in Svalbard, we need to know the concentration of air pollutants generated by a single snowmobile in an effort to evaluate the impact of all vehicles registered and used in Svalbard on local air quality. We focus on the emissions generating ($PM_{2.5}$), of which a two-stroke snowmobile ranges from 0.5 to 1.0 grams per kilometer, whereas four-stroke models lead to 0.1 to 0.2 grams per kilometer see [16]. We performed in-field measurements of ($PM_{2.5}$) generated by snowmobiles used in Svalbard (see Figures 1). The measurements were taken on 17/03/2024 using a Yamaha Venture Lite 600cc snowmobile and Airly air quality sensor (see Fig. 1) starting at 10:30 AM of Svalbard local time in 10-second intervals. The Airly sensor, used in our experiment, is a multi-pollutant air quality monitoring device that provides real-time measurements of gases (CO, NO_2, O_3 and SO_2) and $PM_{1.0}$, ($PM_{2.5}$) and PM_{10} mass concentrations, and environmental parameters such as pressure, temperature, and relative humidity. These sensors count suspended particles of 0.3, 0.5, 1.0, 2.5, 5.0 and 10 μm [15]. The results of the measurements are presented in Fig. 2. As one may see, there is a significant peak while the snowmobile was speeding up when the concentration reached up to 250 $\mu g/m^3$. After that, when the vehicle was driving with constant velocity, the concentration of ($PM_{2.5}$) measured oscillated between 0.9 and around $5\mu g/m^3$. Finally, the concentration increased up to around $20 - 30\mu g/m^3$, which was related to keeping the working vehicle in one place.

3 Hypergraph grammar-based mesh refinements

In this section, we express the 3D longest-edge refinement algorithm by hypergraph-grammar productions. We consider a 3D mesh with tetrahedral elements. We employ the concept of a hypergraph to model the computational mesh. In the hypergraph, we have the hyperedges that connect multiple vertices. The tetrahedra in the hypergraph are represented by vertices modeled as hypergraph nodes attributed by v. The tetrahedral edges are represented as hyperedges connecting

ICCS Camera Ready Version 2025
To cite this paper please use the final published version:
DOI: 10.1007/978-3-031-97635-3_42

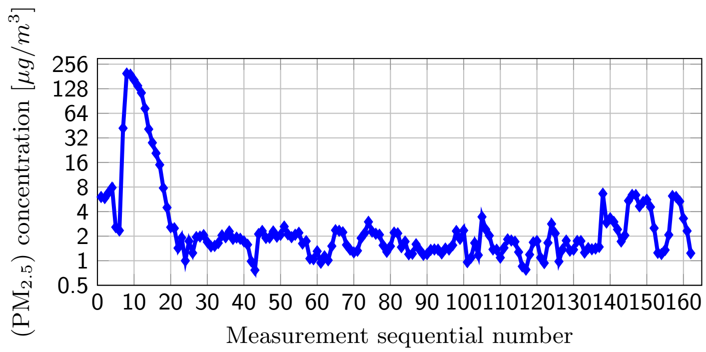

Fig. 2: $(\mathrm{PM}_{2.5})$ concentration generated by snowmobile by 160 measurements performed in 10 seconds intervals in Svalbard on 17/03/2024

two vertices, and they are attributed by E. The tetrahedral faces are modeled as hyperedges connecting three vertex nodes, and they are attributed by F. The tetrahedral interiors are modeled as hyperedges connecting four vertex nodes, and they are attributed by I. The hyperedges denoting the mesh edges have attributes $L{=}L_i$ denoting the length of the edge.

The rules for transforming the computational mesh are described by hypergraph transformations, called hypergraph grammar productions. While a large hypergraph represents the entire mesh, we have twelve hypergraph transformations presented in Table 1. For the simplicity of the presentation, we only plot vertices and hyperedges related to mesh edges (we omit the hyperedges related to faces and interiors). We identify the sub-hypergraph from the left-hand side of the transformation, and the right-hand side replaces it. Since the only connections between sub-hypergraphs and the rest of the hypergraph are the vertices, the replacement is straightforward. All our sub-hypergraphs hang on the mesh vertices, denoted by v. Identification and replacement involve locating the affected vertex nodes and replacing the local hypergraphs connecting them. The computationally expensive part is the identification of the left-hand side since many hyperedges are connected to the hypergraph vertices. We have introduced twelve hypergraph grammar productions. The first hypergraph production **(P1)** breaks a tetrahedral element along the longest edge (the edge with attribute $L{=}L3$ that is the longest edge). It breaks the edge into two new edges, breaks the face into two new faces. It introduces a new internal face, and it breaks an interior into two new interiors. The hypergraph transformations are isomorphic with respect to transformations; that is why we assume we can apply the same hypergraph production for sub-hypergraphs oriented in different ways. All the other hypergraph transformations break tetrahedral elements along the longest edge to remove the hanging edges (to eliminate the situation when a tetrahedral element has a broken face). All the transformations break elements along the longest edge to ensure the proper proportions of the elements. The hypergraph

ICCS Camera Ready Version 2025
To cite this paper please use the final published version:
DOI: 10.1007/978-3-031-97635-3_42

Production	Hypergraph transformation	Production	Hypergraph transformation
(P1)	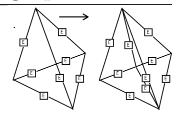	**(P2)**	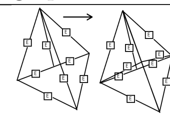
(P3)	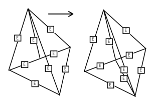	**(P4)**	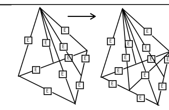
(P5)	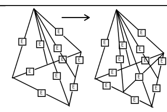	**(P6)**	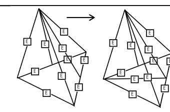
(P7)	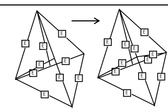	**(P8)**	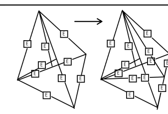
(P9)	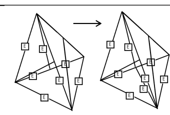	**(P10)**	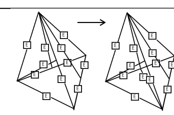
(P11)	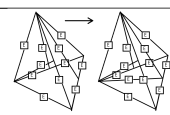	**(P12)**	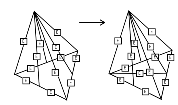

Table 1: Hypergraph grammar productions

productions **(P2)** and **(P3)** consider the longest edge of a tetrahedral element with one face already broken. The hypergraph productions **(P4)**, **(P5)**, **(P6)**, **(P7)** and **(P8)** consider the longest edge of a tetrahedral with two faces already broken. The hypergraph productions **(P9)**, **(P10)**, **(P11)**, and **(P12)** consider the longest edge of a tetrahedral with three faces already broken. There is no case of the tetrahedral with four faces already broken since this case reduces to two tetrahedrons, one with three faces broken or two with two faces broken. Other productions have already expressed these cases.

4 Numerical simulations

In this section we describe computer simulations aimed at modeling the phenomenon of propagation of pollutants generated by the power plant in March 2024. For the wind direction and intensity, as well as vertical profiles of the temperature, we refer to the High-Resolution Operational Forecasts dataset obtained from the National Science Foundation [6] as well as the Global Wind Atlas [4]. We simulated the pollution propagation using the advection-diffusion

To cite this paper please use the final published version:
DOI: 10.1007/978-3-031-97635-3_42

model with the source located at the power plant, on the top of the chimney, assuming the average wind direction and velocity as for the winter season. We have generated the computational mesh using a sequence of hypergraph grammar productions **(P1)** breaking selected finite elements, followed by executions of hypergraph grammar productions **(P2)-(P12)** removing the hanging edges. We generate the computational mesh with tetrahedral elements covering the topography of Svalbard from the GMRT data [14]. To model the power plant chimney accurately, it has been manually incorporated into the initial mesh. The criterion of the tetrahedral element refinement implemented by the hypergraph transformation **(P1)** is the presence of the cross-section of the element with the terrain topography or the chimney. The other hypergraph transformations **(P2)-(P12)** implement the process of the closure of the mesh, to remove hanging edges. We use the weak form of the advection-diffusion equations with Crank-Nicolson time integration scheme stabilized with the SUPG stabilization method [2]:

$$
\begin{aligned}
\left(u_h^{t+1}, v\right) - \frac{dt}{2}\left(\beta_x\left(\frac{\partial u_h^{t+1}}{\partial x}, v_h\right) + \beta_y\left(\frac{\partial u_h^{t+1}}{\partial y}, v_h\right)\beta_z\left(\frac{\partial u_h^{t+1}}{\partial z}, v_h\right)\right.\\
+K_x\left(\frac{\partial u_h^{t+1}}{\partial x}, \frac{\partial v_h}{\partial x}\right) + K_y\left(\frac{\partial u_h^{t+1}}{\partial y}, \frac{\partial v_h}{\partial y}\right) + K_z\left(\frac{\partial u_h^{t+1}}{\partial z}, \frac{\partial v_h}{\partial z}\right)\\
+(R(u_h^{t+1}), \tau\beta\cdot\nabla v_h) = \frac{dt}{2}\left(\beta_x\left(\frac{\partial u_h^{t}}{\partial x}, v_h\right) + \beta_y\left(\frac{\partial u_h^{t}}{\partial y}, v_h\right)\beta_z\left(\frac{\partial u_h^{t}}{\partial z}, v_h\right)\right.\\
\left.+K_x\left(\frac{\partial u_h^{t}}{\partial x}, \frac{\partial v_h}{\partial x}\right) + K_y\left(\frac{\partial u_h^{t}}{\partial y}, \frac{\partial v_h}{\partial y}\right) + K_z\left(\frac{\partial u_h^{t}}{\partial z}, \frac{\partial v_h}{\partial z}\right)\right) + \left(u_h^t, v\right)
\end{aligned} \quad (1)
$$

where $(u,v) = \int_\Omega u(x,y,z;t)v(x,y,z;t)dxdydz$ denotes the L^2 scalar product over the computational domain Ω computed for the time moment t, $R(u) = \frac{\partial u}{\partial x} + \frac{\partial u}{\partial y} + \frac{\partial u}{\partial z} + \epsilon\Delta u$, and $\tau^{-1} = \left(\frac{\beta_x}{h_x} + \frac{\beta_y}{h_y} + \frac{\beta_z}{h_z}\right) + 3\epsilon\frac{1}{h_x^2+h_y^2+h_z^2}$.

In our simulation, we assume $K_x = K_y = 1.0$ and $K_z = 0.01$. As illustrated in Figure 3 the pollution propagates into the valley where Longyearbyen is located. Without strong winds and thermal inversion effects, pollutants cannot be dispersed over large areas, contributing to their stagnation in the valley. Four hours after the chimney starts producing the pollution, the whole valley is filled with pollution (see Figure 3).

Conclusions Computer simulations discussed in the paper show that the combination of emissions of air pollutants with the specific atmospheric and/or terrain conditions, like the one observed in the Longyearbyen region, may result in a stagnation of the pollutants in the valley of Longyearbyen.

The diesel power plant in Longyearbyen, Svalbard, generates approximately 11 megawatts (MW) of electricity. According to data from the North American Commission for Environmental Cooperation [1], PM2.5 emission rates for oil-fired power plants typically range from 0.05 to 0.10 kilograms per megawatt-hour (kg/MWh). Assuming high-quality filters, the diesel power plant in Longyearbyen is estimated to emit an average of $4 \times 0.05 = 0.2$ (kg/MWh) kilograms of PM2.5 per four hours under continuous full-load operation. We selected a four

ICCS Camera Ready Version 2025
To cite this paper please use the final published version:
DOI: 10.1007/978-3-031-97635-3_42

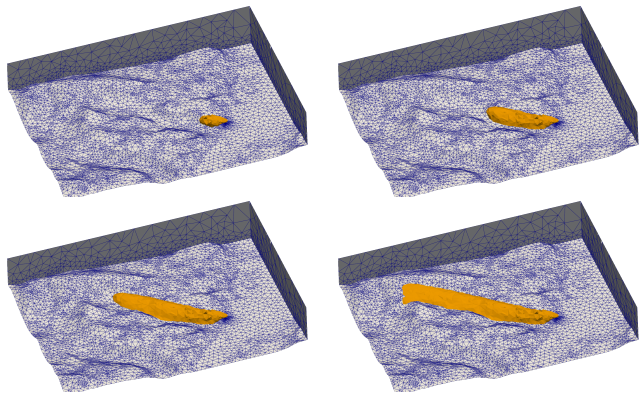

Fig. 3: The front views of the smoke propagated from the chimney into the valley. Half on hour, 90 minutes, 150 minutes, and 210 of power plant operation.

hours interval since this is the time when the pollution distributes uniformly over the entire valley. Due to the topography and wind conditions, this PM2.5 spreads in the valley contributing to an average of 200×10^7 grams per m^3 which results in $200 \times 10^7/10^9 = 2$ (μ g/m^3). This estimate coincides with the measurements from the snowmobiles, oscillating between 0.9 and $5\mu g/m^3$. We can also conclude that the pollution generated from snowmobiles is of the same order as the pollution propagating from the new diesel engines power plant.

Acknowledgements Research project supported by the program "Excellence Initiative - Research University" for the AGH University of Science and Technology. The research presented in this paper was partially supported by the funds of Polish Ministry of Science and Higher Education assigned to the AGH University of Krakow. The work of Albert Oliver-Serra was supported by "Ayudas para la recualificación del sistema universitario español" grant funded by the ULPGC, the Ministry of Universities by Order UNI/501/2021 of 26 May, and the European Union-Next Generation EU Funds. The Authors gratefully acknowledge the support and assistance of The Polish Polar Station Hornsund for help with data collection.

References

1. North American Power Plant Air Emission https://www.cec.org/sites/default/napp/en/particulate-matter-emissions.php
2. Brooks, A.N., Hughes, T.J.: Streamline upwind/Petrov-Galerkin formulations for convection dominated flows with particular emphasis on the incompressible Navier-Stokes equations. Computer Methods in Applied Mechanics and Engineering **32**(1), 199–259 (1982)
3. Charles, D.: A 'forever' seed bank takes root in the Arctic. Science **312**(5781), 1730–1731 (2006)

DOI: 10.1007/978-3-031-97635-3_42

4. Davis, N.N., Badger, J., Hahmann, A.N., Hansen, B.O., Mortensen, N.G., Kelly, M., Larsén, X.G., Olsen, B.T., Floors, R., Lizcano, G., Casso, P., Lacave, O., Bosch, A., Bauwens, I., Knight, O.J., van Loon, A.P., Fox, R., Parvanyan, T., Hansen, S.B.K., Heathfield, D., Onninen, M., Drummond, R.: The Global Wind Atlas: A high-resolution dataset of climatologies and associated web-based application. Bulletin of the American Meteorological Society **104**(8), E1507 – E1525 (2023)
5. Dekhtyareva, A., Hermanson, M., Nikulina, A., Hermansen, O., Svendby, T., Holmén, K., Graversen, R.G.: Springtime nitrogen oxides and tropospheric ozone in Svalbard: results from the measurement station network. Atmospheric Chemistry and Physics **22**(17), 11631–11656 (2022)
6. European Centre for Medium-Range Weather Forecasts: ECMWF IFS High-Resolution Operational Forecasts (2016). https://doi.org/10.5065/D68050ZV, https://rda.ucar.edu/datasets/d113001/, accessed: 2024-11-25
7. Paszyńska, A., Paszyński, M., Grabska, E.: Graph transformations for modeling hp-adaptive finite element method with triangular elements. In: Proceedings of the 8th International Conference on Computational Science, Part III. p. 604–613. ICCS '08, Springer-Verlag, Berlin, Heidelberg (2008). https://doi.org/10.1007/978-3-540-69389-5_68, https://doi.org/10.1007/978-3-540-69389-5_68
8. Paszyńska, A., Paszyński, M., Grabska, E.: Graph transformations for modeling hp-adaptive finite element method with mixed triangular and rectangular elements. In: Proceedings of the 9th International Conference on Computational Science. p. 875–884. ICCS 2009, Springer-Verlag, Berlin, Heidelberg (2009). https://doi.org/10.1007/978-3-642-01973-9_97, https://doi.org/10.1007/978-3-642-01973-9_97
9. Paszyński, M.: On the parallelization of self-adaptive hp-finite element methods. part I. Composite Crogrammable Graph Grammar model. Fundamenta Informaticae **93**(4), 411–434 (2009)
10. Paszyński, M.: On the parallelization of self-adaptive hp-finite element methods. part II. Partitioning Communication Agglomeration Mapping (pcam) analysis. Fundamenta Informaticae **93**(4), 435–457 (2009)
11. Podsiadło, K., Serra, A.O., Paszyńska, A., Montenegro, R., Henriksen, I., Paszyński, M., Pingali, K.: Parallel graph-grammar-based algorithm for the longest-edge refinement of triangular meshes and the pollution simulations in lesser poland area. Engineering with Computers **37**, 3857–3880 (2021)
12. Rivara, M.C.: Algorithms for refining triangular grids suitable for adaptive and multigrid techniques. International Journal Numerical Methods in Engineering **20**(4), 745–756 (1984)
13. Rivara, M.C.: Mesh refinement processes based on the generalized bisection of simplices. SIAM Journal Numerical Analysis **21**(3), 604–613 (1984)
14. Ryan, W.B.F., Carbotte, S.M., Coplan, J.O., O'Hara, S., Melkonian, A., Arko, R., Weissel, R.A., Ferrini, V., Goodwillie, A., Nitsche, F., Bonczkowski, J., Zemsky, R.: Global multi-resolution topography synthesis. Geochemistry, Geophysics, Geosystems **10**(3) (2009)
15. South Coast Air Quality Management District: Airly sensor detail (2024), https://www.aqmd.gov/aq-spec/sensordetail/airly, accessed: 2024-11-25
16. U.S. Department of the Interior, National Park Service: Scientific assessment of Yellowstone National Park winter use March 2011, https://npshistory.com/publications/yell/winter-use-sci-assessment-2011.pdf

ICCS Camera Ready Version 2025
To cite this paper please use the final published version:
DOI: 10.1007/978-3-031-97635-3_42